Bifurcation of ensemble oscillations and acoustic emissions from early stage cavitation clouds in focused ultrasound

2013 New J. Phys. 15 033044

(http://iopscience.iop.org/1367-2630/15/3/033044)

New Journal of Physics
The open access journal for physics

Bifurcation of ensemble oscillations and acoustic emissions from early stage cavitation clouds in focused ultrasound

Bjoern Gerold[1], **Itay Rachmilevitch**[2] **and Paul Prentice**[1,3,4]
[1] Institute for Medical Science and Technology, University of Dundee, Dundee DD2 1FD, UK
[2] InSightec Ltd, Tirat Carmel 39120, Haifa, Israel
[3] Department of Physics, University of Dundee, Dundee DD1 4HN, UK
E-mail: p.prentice@dundee.ac.uk

New Journal of Physics **15** (2013) 033044 (16pp)
Received 17 December 2012
Published 28 March 2013
Online at http://www.njp.org/
doi:10.1088/1367-2630/15/3/033044

Abstract. The acoustic emissions from single cavitation clouds at an early stage of development in 0.521 MHz focused ultrasound of varying intensity, are detected and directly correlated to high-speed microscopic observations, recorded at 1×10^6 frames per second. At lower intensities, a stable regime of cloud response is identified whereby bubble-ensembles exhibit oscillations at half the driving frequency, which is also detected in the acoustic emission spectra. Higher intensities generate clouds that develop more rapidly, with increased nonlinearity evidenced by a bifurcation in the frequency of ensemble response, and in the acoustic emissions. A single bubble oscillation model is subject to equivalent ultrasound conditions and fitted to features in the hydrophone and high-speed spectral data, allowing an effective quiescent radius to be inferred for the clouds that evolve at each intensity. The approach indicates that the acoustic emissions originate from the ensemble dynamics and that the cloud acts as a single bubble of equivalent radius in terms of the scattered field. Jetting from component cavities on the periphery of clouds is regularly

[4] Author to whom any correspondence should be addressed.

observed at higher intensities. The results may be of relevance for monitoring and controlling cavitation in therapeutic applications of focused ultrasound, where the phenomenon has the potential to mediate drug delivery from vasculature.

S Online supplementary data available from stacks.iop.org/NJP/15/033044/mmedia

Contents

1. Introduction **2**
2. Experimental arrangement **3**
2.1. The sonoptic chamber . . . 3
2.2. Passive cavitation detector . . . 4
3. Experimental results **5**
3.1. High-speed observations . . . 5
3.2. Acoustic detection . . . 7
3.3. Jetting from peripheral bubbles . . . 9
4. Analysis **9**
4.1. Single bubble Rayleigh–Plesset model . . . 9
4.2. Rayleigh–Plesset robustness analysis . . . 12
5. Conclusions **13**
Acknowledgments **13**
Appendix. Assumption of HIFU nonlinearity **14**
References **15**

1. Introduction

Acoustic cavitation refers to the formation of bubbles and bubble-ensembles in a medium subjected to the pressure fluctuations of an intense sound field. The phenomenon is known to have a pivotal role in applications such as sonochemistry [1], material erosion [2] and acoustic cleaning [3]. Cavitation is often detected acoustically through the use of a hydrophone device, data from which can be analysed for information regarding the nature of the cavitation activity, such as stable versus inertial behaviour ([4, chapter 4]). A seminal experimental study on this topic by Lauterborn and Cramer [5], reported a 'sub-harmonic route to acoustic chaos', whereby emission spectra with sub-harmonic features to the driving frequency, f_0 of 22.56 kHz, bifurcate to odd sub-harmonics given by $nf_0/3$ and $nf_0/8$ lines, then $nf_0/4$ lines, with increasing drive amplitude. At a sufficiently high amplitude, the spectrum was dominated by chaotic broadband noise associated with inertial cavitation, although distinct spectral features remained apparent. The nonlinear response of single bubbles exposed to periodic pressure fluctuations, has received comprehensive theoretical treatment (see e.g. [6, 7]).

Cavitation activity can also be directly observed and analysed with high-speed photography. Due to framing-rate limitations, the majority of the literature available on high-speed observation of cavitation cloud and bubble-ensemble dynamics, has been undertaken within ultrasound cleaning baths or with vibrating horns, typically driven at several tens of kHz and often in standing wave configurations [8–10]. Moreover, the stochastic nature of cavitation

nucleation limits observations to steady state conditions, when clouds have become established and adopted quasi-stable, periodic behaviour in response to applied insonation.

High intensity focused ultrasound (HIFU) refers to the minimally-invasive application of ultrasound in the MHz range, for the administration of therapy to targeted diseased tissue. Cavitation is a common occurrence at the intensities typically employed and is the subject of a substantial research effort, seeking to exploit its potential to enhance therapeutic effects [11]. This includes inertial activity, which is characterized by broadband acoustic emissions and stable cavitation, identified by harmonic frequency content, for the delivery of therapeutic agents to tissue via extravasation and tissue permeabilization, [12, 13], respectively. The latter often employs shelled contrast agent microbubbles, delivered via intra-vasculature injection, to provide cavitation nuclei *in vivo*. Realization of the potential for HIFU-mediated, cavitation-enhanced therapy is somewhat hindered by a deficit in the fundamental understanding of cavitation cloud evolution in MHz propagating focused ultrasound, particularly over the first few hundred cycles of exposure. The introduction of controlled cavitation to tissue for enhanced therapy would further demand a mechanism through which activity can be monitored, to ensure localization to the target region. As acoustic cavitation in HIFU typically evolves extremely rapidly, detection from inception and through the early stages of cloud development is critical, to avoid unwanted collateral damage to surrounding healthy tissue.

We have recently developed a laser-nucleation technique to predetermine the onset of acoustic cavitation activity in HIFU, permitting interrogation at unprecedented spatial and temporal resolution [14]. Here, we report on the observation of bubble-ensemble dynamics during the formative phases of development in water, systematically studied under HIFU exposure across a range of typical therapeutic intensities, for the first time. Furthermore, a passive cavitation detector (PCD) was constructed, based on a series of preliminary high-speed imaging experiments, sensitive at frequencies matching the bandwidth of the observed ensemble oscillations, for parallel acoustical monitoring temporally resolved to the duration of observation. Analysis of cloud response to HIFU insonation is conducted via three approaches: the sub-harmonic frequency content of the acoustic emissions detected, which is compared to model oscillations of a single bubble of selected quiescent radius comparable to that of the cloud, and the response behaviour of the bubble-ensemble dynamics, extracted from the high-speed microscopic imaging sequences.

The results correlate acoustic emissions directly to resolved, early stage cloud dynamics in HIFU. The analysis suggests that the physical size of a cloud can be inferred from the spectra of the scattered field, for a given set of HIFU parameters, via a simple single bubble model.

2. Experimental arrangement

2.1. The sonoptic chamber

The 'sonoptic' chamber is custom-built to accommodate the focused ultrasound field of a 100 mm diameter, spherically focused HIFU transducer, without reflection or scatter [14], impedance-matched to a drive frequency, $f_0 = 0.521$ MHz. Pressure maps measured with a fibre-optic hydrophone (Precision Acoustics) through the focal, near- and far-fields, in both the sonoptic chamber and a free-field scanning tank ($1 \times 1 \times 1\ \mathrm{m}^3$) configuration, confirmed this to be the case. The device is driven with a sinusoidal signal from a waveform generator (Agilent 33250A) passed through a power amplifier (ENI 3200L). HIFU intensities of peak negative pressure (PNP) amplitude between ~0.7 MPa (the lowest value at which cavitation

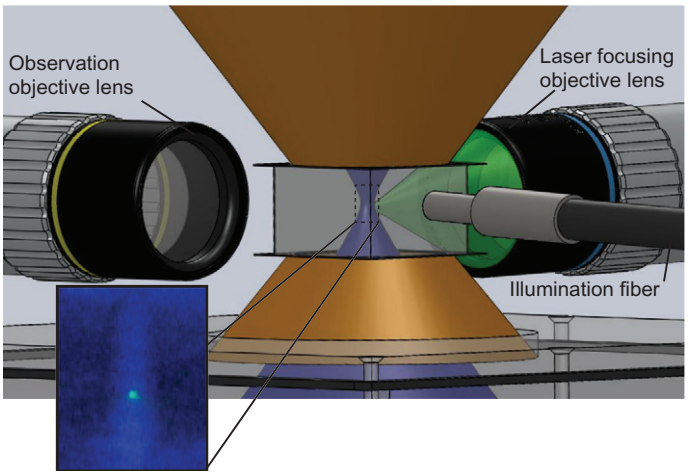

Figure 1. Schematic representation of the cavitation chamber, accommodating the focus of the HIFU field (represented blue) which propagates upwards from a source transducer located on the base of the sonoptic chamber. The laser-pulse (represented green) is focused through a long working distance objective lens. Alignment is achieved via schlieren imaging of the HIFU focus (inset bottom left) and translation of the laser focus (green spot) through manual scanning of the focusing objective lens. High-speed imaging is undertaken through a second orthogonal objective lens, opposite which a fibre-optic bundle provides flash-illumination.

clouds can be reliably nucleated) and 1.3 MPa are investigated. The focal region of the HIFU field is contained within a glass cavitation chamber, figure 1, which facilitates optical access for microscopic observation and pulsed laser irradiation, through long working distance objective lenses (Mitutoyo 20×0.28 NA and 50×0.42 NA, respectively). High-speed imaging is undertaken with a Shimadzu HPV-1 camera, recording 100 frames (312×260 pixels) at 1×10^6 frames per second (Mfps), with an individual exposure time of 0.25 μs. Illumination is achieved with a flash lamp coupled to a fibre-optic bundle via a condenser lens.

Acoustic cavitation is nucleated via a 6–8 ns 532 nm laser-pulse (Nano S 130–10 frequency-doubled Q-switched Nd:YAG, Litron Lasers) of energy 0.9 ± 0.1 mJ, incident to the focal region of a pre-established HIFU field. Crucially, this is below the breakdown threshold for the host medium of de-ionized water, degassed to an O_2 content below 4 mg l^{-1}, which avoids the comparatively large plasma-mediated vapour bubble, generally associated with pulsed laser-induced cavitation research [15, 16]. A total of 160 HIFU acoustic cycles are generated, with the laser-pulse incident after 80 μs, to allow for transducer 'ring-up' to the required pressure amplitude. High-speed camera operation is triggered to capture a few frames prior to nucleation of cavitation activity, such that cloud development is observed from inception through ~50 HIFU cycles.

2.2. Passive cavitation detector

The PCD is fabricated from piezo-ceramic composite, measuring $9 \times 9 \times 3$ mm^3, cut with kerfs to improve response efficiency and reduce lateral modes. The large active area of the device

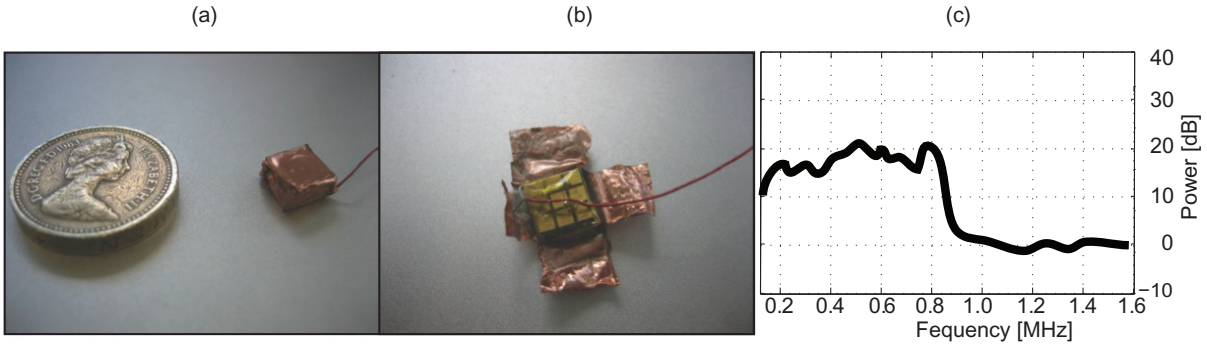

Figure 2. (a) The PCD used to detect acoustic emissions from cavitation clouds in focused ultrasound. (b) With the copper tape peeled back to reveal the kerfed piezo-ceramic composite. (c) Sensitivity characteristic for PCD.

provides a high sensitivity to a frequency bandwidth related to its thickness. Silver epoxy provided the acoustic matching and acted as an electrode to the element. Copper tape provided the ground and shielded the device, particularly from the Q-switch of the pulsed laser. A second electrode is soldered to micro-coaxial cable and isolated from the shielding. A photograph of the device is provided, figures 2(a) and (b).

The sensitivity of the device was determined by positioning the PCD in a water tank at ∼1 m from the field of a HIFU field, in degassed water. A transducer (ExAblate 2000, InSightec Ltd) was driven at a very high power to generate cavitation, which could be observed visually and produced a characteristic 'fizzing' sound in the audible range. A 1 ms signal was recorded several times for analysis in MATLAB. Three recordings in the frequency domain were averaged and the 1.17 MHz driving frequency filtered out. In this manner a sensitivity characteristic, as depicted in figure 2(c), was obtained following the boundary of the acoustic spectra.

During an experiment the PCD is positioned within the sonoptic chamber, a few millimetres from the acoustic focus, connected to an oscilloscope (Agilent MS07104A). Data is recorded at a minimum of 1 GS s^{-1}, saved in .bin format on an USB stick and transferred to a PC for subsequent analysis.

3. Experimental results

3.1. High-speed observations

Figures 3(a) and (b) are sample high-speed imaging data illustrating cloud behaviour in response to HIFU of PNP $= 0.72 \pm 0.13$ (instrument error, according to manufacturer) and 1.04 ± 0.18 MPa, respectively. These are sequential images acquired over a duration of 12 μs, approximately 75 μs following laser-nucleation, during which the cloud has become established and initiated periodic behaviour. Slight upward translation is attributable to the acoustic radiation force of the HIFU insonation, as buoyancy is negligible over the timescale of the observations. Inspection indicates that the quiescent component bubble radius is comparable for both clouds, as expected for acoustic cavitation at a given driving frequency [4, 11, 17].

Both coalescence of component bubbles during expansion, and fragmentation after collapse, within the clouds is observed. The latter is the mechanism by which the number of

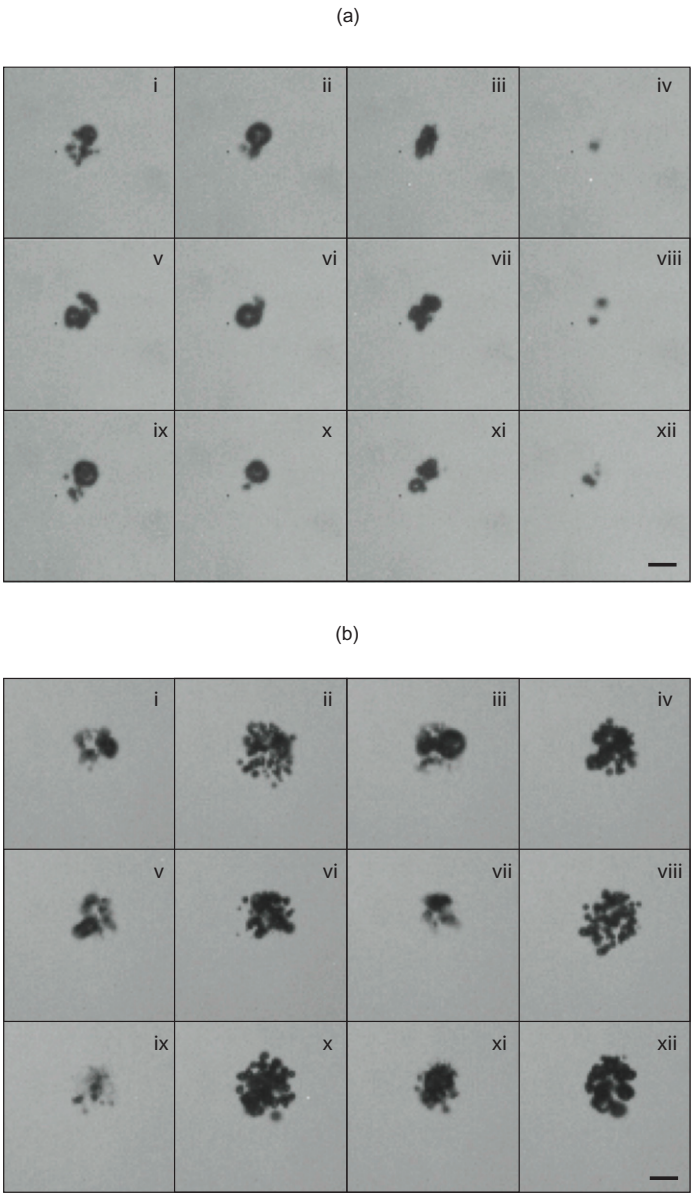

Figure 3. Consecutive frames extracted from high-speed sequences recorded at 1 Mfps, of cavitation clouds evolving in HIFU in a (a) stable regime at PNP = 0.72 MPa and (b) more pronounced nonlinear regime at PNP = 1.04 MPa, ∼75 μs following the laser-nucleation event. Scale bar bottom right: 50 μm.

constituent bubbles increases, at a rate dependent on the intensity of the HIFU field. Several tens of μs following laser-nucleation, quasi-spherical breathing mode oscillations for the bubble-ensembles, closely related to the dynamics of the individual component bubbles, are apparent. The effect is particularly evident towards the latter stages of the movie representation of the high-speed sequences sampled for figures 3(a) and (b), available as supplementary material (from stacks.iop.org/NJP/15/033044/mmedia)[5]. It is well known that oscillating bubbles exert either mutually attractive or repulsive forces via coupling to the radiated acoustic field of other

[5] Supplementary material: high-speed sequence in movie format (at full image size acquired by camera).

bubbles in the vicinity, or secondary Bjerknes effects [18]. However, due to the proximity of the component bubbles within the clouds generated, figure 3, we attribute the ensemble dynamics to the combined effect of the constituent bubbles, through the physical action of individual bubble oscillations. For example, the collapse of any individual bubble will act to draw its nearest neighbours closer, which when extended to all the bubbles within the population oscillating in phase, generates an overall compression for the cloud.

Figures 3(a)(iv), (viii) and (xii) depict consecutive compressive phases, for the cloud at lower PNP, with approximately one HIFU cycle propagating during the time taken to acquire two high-speed images. This constitutes an ensemble response at $f_0/2$, the half-harmonic of the driving frequency, also known as period-doubling [4–7].

Figure 3(b) is the equivalent high-speed data for a cloud nucleated at higher PNP, whereby a larger bubble-ensemble has developed due to increased levels of fragmentation over the preceding 75 μs. As well as the HIFU intensity-dependent size of the clouds of figures 3(a) and (b), a further notable difference is the additional deflation phases, captured in figures 3(b)(i), (iii), (v), (vii), (ix) and (xi). The full sequence recorded for the cloud at higher PNP, available in movie format as supplementary material (see footnote 5), clearly illustrates the ensemble pulsating at more than one frequency.

To quantify the ensemble oscillations, a dark-pixel counting algorithm is implemented to each of the 100 images captured within a high-speed sequence. This effectively yields a 'summed bubble area' variation with time, for every observation of cloud evolution at each PNP investigated. This approach does not explicitly distinguish between ensemble response and constituent bubble dynamics. However, for the high void-fraction clouds being investigated, constituent bubble dynamics and ensemble response are synonymous, as discussed previously. The application of a fast Fourier transform (FFT) to the summed bubble area–time curve from each sequence, is thereby taken to provide the frequency of the ensemble oscillations, at the given HIFU PNP. The resulting high-speed sequence (HSS) spectra for the clouds of figures 3(a) and (b) are presented in figure 4 below, for direct comparison to the frequency content of the acoustic emissions collected from these clouds, specifically. A summary of all experimentally detected acoustic and HSS spectral data is provided in figure 7 below.

3.2. Acoustic detection

The acoustic emissions from individual clouds are detected for the duration of high-speed observation, via the PCD device described above. Figure 4(a) is an FFT of a PCD recording of the primary HIFU field at PNP = 1.04 MPa, without the nucleation of cavitation activity (i.e. no laser-pulse incident). The fundamental driving frequency at $f_0 = 0.521$ MHz is the dominant feature, with a smaller peak at $2f_0$, the second harmonic. The potential influence of the higher harmonics on the cavitation cloud behaviour is discussed (see the appendix) below.

The green traces of figures 4(b) and (c) are the spectra of the acoustic emissions collected for the clouds of figures 3(a) and (b), respectively. The sub-fundamental peaks (arrowed black) are only detected when cavitation activity is nucleated with a laser-pulse, with structure detail dependent on the PNP of the HIFU field driving the activity. As such, we refer to the frequency of these features as emitted frequencies, f_e. The cloud at lower intensity exhibits $f_e \approx 260$ kHz (7 kHz full-width at half-maximum (FWHM); acoustic data), which corresponds to the $f_0/2$ sub-harmonic. Figure 4(c) reveals spectral lines at $f_e \approx 175$ (40 kHz FWHM) and 350 kHz (30 kHz FWHM), which correspond to $f_0/3$ and $2f_0/3$, respectively, emitted from the cloud

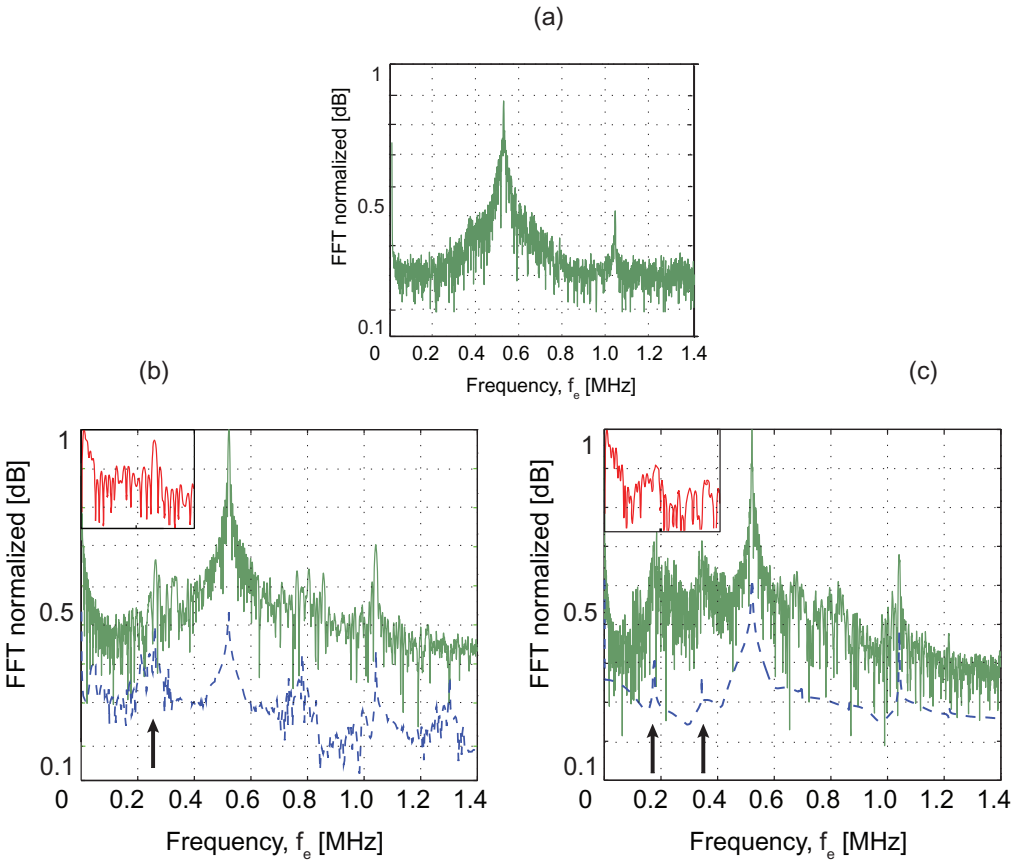

Figure 4. (a) Control experiment with no cavitation activity nucleated, depicting the PCD detection of the primary HIFU field. Panels (b) and (c) are FFTs of the PCD signal (green) collected from the clouds of figures 3(a) and (b), respectively. The inset (red, at same frequency scale) represents the ensemble dynamics deduced from a FFT of the dependence of 'summed bubble area' (dark pixel count) on time, throughout the high-speed imaging sequence. An FFT of the RP radius-time curves for a single bubble of selected R_0 (blue dash), under equivalent ultrasonic conditions is also presented, described (see section 4.1).

depicted in figure 3(b). The frequency-bifurcation in the ensemble dynamics and acoustic emissions at higher intensities represents a transition into a regime of increased nonlinear response for the cloud-system, a phenomenon which, for single bubbles, has previously received theoretical attention [6, 7].

Also depicted in figures 4(b) and (c) are the HSS spectra (red trace inset) obtained from the dark pixel counting algorithm applied to the entire sequence of figures 3(a) and (b), as described. The signal resolution for this analysis is inherently limited by the number of samples available (100 frames per high-speed sequence). Moreover, the frequency of oscillation signal will only become available once the cloud has entered its periodic response phase, typically 20–30 μs following the initial nucleation event. Nonetheless, excellent agreement between the frequency content of the acoustic emissions and ensemble dynamics is apparent. Finally, model spectra (blue dash) from a Rayleigh–Plesset (RP) formulation for single bubble oscillation at selected values of R_0 are also presented, as discussed (see section 4.1) below.

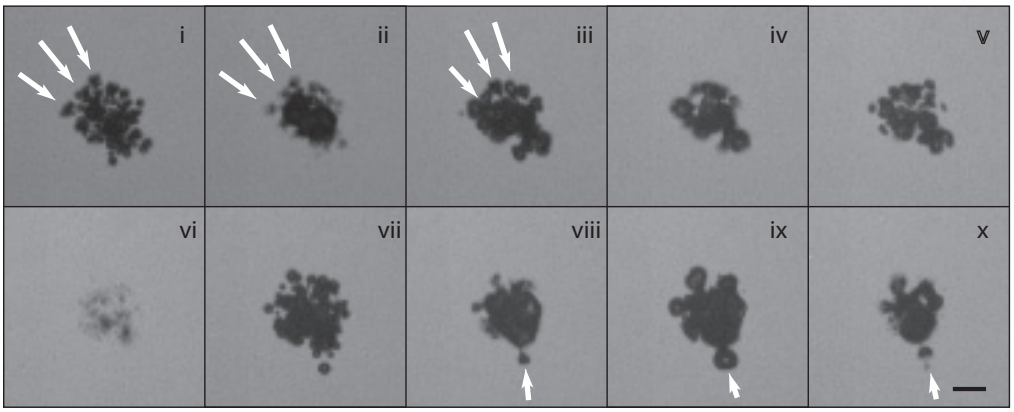

Figure 5. Sequential frames extracted from ~80 μs after the nucleation event, in HIFU of PNP = 1.29 MPa, rich in jetting activity from bubbles peripheral to the cloud (examples arrowed white). Scale bar bottom right: 50 μm.

3.3. Jetting from peripheral bubbles

The increased nonlinearity of the ensemble dynamics at higher PNPs is underscored by frequent observation of jet, and counter-jet formation [19], from bubbles on the periphery of the clouds, figure 5; a number of examples are arrowed white. Inwardly directed jetting from bubbles that formed at hydrophobic pits, etched in a two-dimensional array on a surface has been reported before [20], albeit under comparatively controlled and idealized conditions. To the best of our knowledge, the observations of figure 5 represent the first at sufficient temporal and spatial resolution to identify jets from bubbles at the periphery of a cloud, that are constituent to it, particularly at a typical HIFU driving frequency. Jetting activity was not been observed at HIFU PNPs < 1.0 MPa.

4. Analysis

4.1. Single bubble Rayleigh–Plesset model

To investigate the origin of the emitted acoustic frequency content, we implement a RP formulation for a single bubble [4, 7, 21] given as equation (1). This form of analysis for cloud breathing modes has been undertaken previously for the central region of a 'streamer' in the standing field of an acoustic cleaning bath [7]. A remarkable degree of agreement between the time-varying radius of the cloud, observed at 0.1 Mfps at a driving frequency of 12.96 kHz, and those obtained from an RP formulation was demonstrated. Accordingly, we present our experimental results in parallel with equivalent model predictions, for an R_0 selected such that the features of the frequency spectrum of the single bubble model oscillations match those observed for the bubble-ensembles, through the HSS spectrum and those detected within the acoustic emissions, figures 4(b) and (c):

$$R\ddot{R} + \frac{3\dot{R}^2}{2} = \frac{1}{\rho}\left\{\left(p_0 + \frac{2\sigma}{R_0} - p_v\right)\left(\frac{R_0}{R}\right)^{3\kappa} + p_v - \frac{2\sigma}{R} - \frac{4\eta\dot{R}}{R} - p_0 - P\,(t)\right\}, \tag{1}$$

where R is the time-varying radius of the bubble undergoing oscillation and R_0 is as elected quiescent radius, $p_0 = 100\,\text{kPa}$ is the hydrostatic pressure, $p_v = 2.33\,\text{kPa}$ and $\kappa = 5/3$ are the vapour pressure and polytropic exponent of the gas within the bubble. $\rho = 10^3\,\text{kg m}^{-3}$, $\sigma = 72 \times 10^{-3}\,\text{N m}^{-1}$ and $\eta = 0.894 \times 10^{-3}\,\text{Pa s}$ are the density, surface tension and liquid viscosity of the host medium, respectively. $P(t)$ represents the HIFU excitation, given the form

$$P(t) = \text{PNP} \sin(2\pi f_0 t) \tag{2}$$

at frequency f_0 and PNP amplitude, matching those of the experiments. An analysis of the appropriateness of using a linear expression for the HIFU insonation, is provided below (see the appendix).

Specifically, quiescent R_0 radii are implicated by fitting RP model sub-fundamental spectral features to the measured emitted frequencies, for each PNP investigated. Example model spectra from this approach are presented (blue dash) in figures 3(b) and (c), whereby R_0 of 20.2 and 26.3 μm yield sub-fundamental structure at f_e of 260 kHz for a PNP of 0.72 MPa, and 175 and 350 kHz for 1.04 MPa (at $f_0 = 0.521$ MHz). A robustness analysis confirms that variation (including in combination) of the other parameters of equation (1) is unlikely to deliver spectral features that resemble those experimentally observed. Sample analysis results for variation of host medium viscosity, η and surface tension, σ are available (see section 4.2) below.

The dependence of the model R_0 required to deliver the experimental spectra structure on HIFU PNP, is given in figure 6. The PNP amplitude is both an input parameter to the RP model via the HIFU excitation expression of equation (2), and the experimental factor that determines the rate of fragmentation within the bubble ensemble, and therefore the time-averaged size of the observed clouds.

It is not possible to deduce a quiescent radius for the clouds explicitly from the high-speed sequences. For comparative purposes however, approximations of maximum and minimum cloud radii are also represented, figure 6, using the highest and lowest values of the dark pixel count, averaged over all the high-speed sequences acquired at each PNP investigated. During this process, dark pixels are rearranged into a circle, to homogenize cloud morphologies and effectively assume a void fraction of $\sim$1, which is reasonable for the ensemble at maximal expansion. The approximation for the minimum cloud radius should not be interpreted literally as some of the collapsed constituent bubbles within the ensemble are likely to be below the imaging resolution for the high-speed camera set-up. Nonetheless, the comparison between the experimental radii approximations and the single bubble model R_0, which were coupled through the PCD spectra for the acoustic emissions, is compelling, and may be taken to indicate that the frequency content of the acoustic emissions originate from the response of the cloud, acting as a bubble-ensemble.

Figure 7 represents an overview of the experimental acoustic and HSS, and RP model, spectral information obtained for each PNP investigated. The bifurcation of f_e, both in terms of the emitted acoustic frequencies and the ensemble oscillations, at PNP ≈ 0.78 MPa is clearly visible. The blue dot region represents sub-fundamental RP model oscillation frequencies matched to the experimentally detected f_e values, which agrees well with both the bifurcation PNP threshold, and the degree of frequency splitting throughout the bifurcation transition.

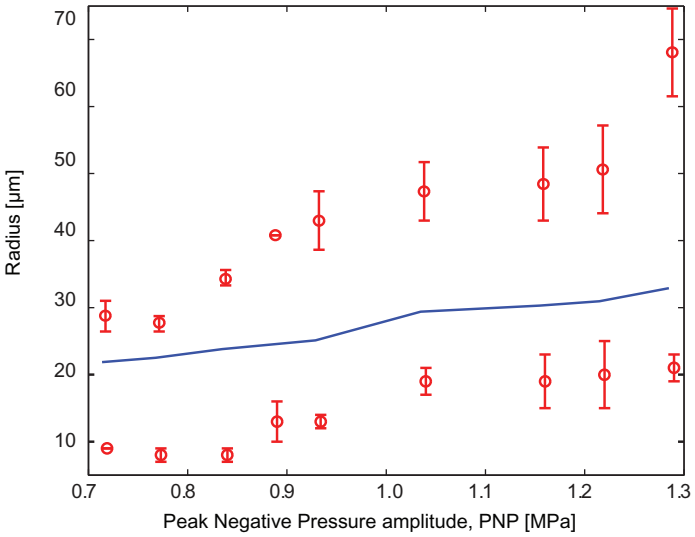

Figure 6. Variation of model R_0 with PNP amplitude (solid blue line) required to yield frequency content from the RP model oscillations matching those emitted from the cavitation clouds, detected with the PCD. The experimental data (red circles) depicts the maximum and minimum radii approximations for the clouds, as discussed in the text. Error bars are standard deviation for the approximate cloud size at each PNP ($n \geqslant 6$).

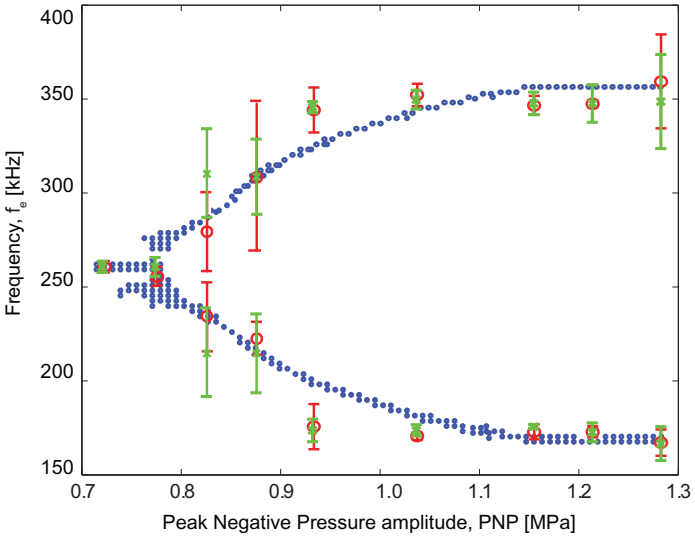

Figure 7. Summary of all experimental frequency content information obtained, including PCD detection of acoustic emissions (green) and HSS analysis of ensemble oscillation dynamics (red), for each of the eight PNPs investigated. Error bars are the standard deviation for each data set, with $n \geqslant 6$. The blue dots represent the spectral features above a threshold value derived from the RP model, fitted with selected values of R_0 (see figure 6).

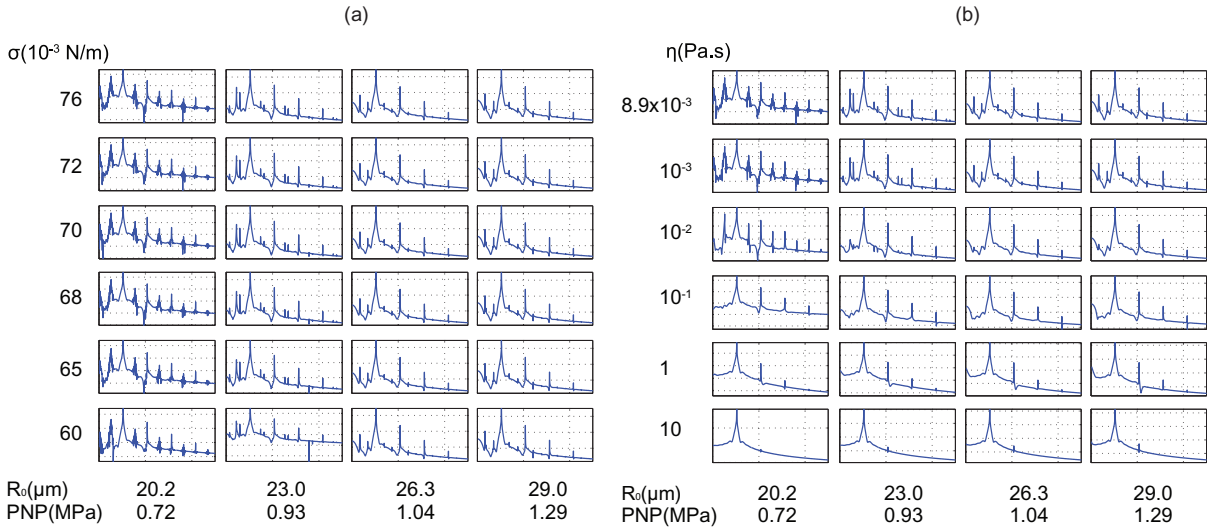

Figure 8. (a) Robustness analysis for surface tension, σ ranging from 60×10^{-3} to 76×10^{-3} N m^{-1}, over the values of selected R_0 and PNP of interest. (b) Robustness analysis for liquid viscosity, η ranging from 8.9×10^{-3} to 10^3 Pa s. Power (dB) spectra are presented in the range of 0–2.5 MHz.

4.2. Rayleigh–Plesset robustness analysis

To ensure the sub-fundamental spectral features could not arise from the variation of parameters (including in combination) in the RP model for single bubble dynamics, other than R_0 for a given HIFU PNP amplitude, a robustness analysis is conducted.

For brevity, matrices of model spectra are presented for the R_0 and PNPs of interest, through parameter space for surface tension σ, and liquid viscosity η, figures 8(a) and (b), respectively, are presented to demonstrate proof-of-principle. A short discussion on the relevance of the parameters to the observations follows.

The surface tension of a liquid is related to its temperature, such that the range presented corresponds to water from 0 °C ($\sigma = 76 \times 10^{-3}$ N m^{-1}) to 100 °C ($\sigma = 58 \times 10^{-3}$ N m^{-1}). Although collapsing cavities are known to generate high core temperatures, including in multi-bubble configurations [2], the energy is very localized both spatially and temporally, to the location and moment of collapse. We therefore assume room temperature of 25 °C and thus surface tension, $\sigma = 72 \times 10^{-3}$ N m^{-1}, for equation (1).

Increasing the host medium viscosity acts to suppress the amplitude of all spectral features, figure 8(b), as expected. In the extremity, where $\eta = 10$ Pa s, the model single bubble predominantly oscillates at the fundamental driving frequency, $f_0 = 0.521$ MHz, irrespective of R_0 or PNP. The viscosity of tissue is often approximated to that of glycerol, $\eta_{gl} \approx 1.5$ Pa s [22]. However, whole blood has viscosity, $\eta_{wb} \approx 4 \times 10^{-3}$ Pa s [23], a region of parameter space for which the sub-fundamental frequency structure is apparent across the full range of R_0 and PNP reported. As such, the signature acoustic emissions identified may have application for cavitation clouds forming within the vasculature, under HIFU exposure.

5. Conclusions

We present temporally resolved and directly correlated optical observations and acoustic recordings, of single cavitation clouds developing at a very early stage of evolution in focused ultrasound, for the first time. The frequency of the physical bubble-ensemble oscillations translate directly to frequency content within the acoustic emissions, detectable via hydrophones custom-fabricated for sensitivity over the required bandwidth.

The analysis undertaken does not distinguish between the individual constituent bubble dynamics within the cloud, and the dynamics of the cloud itself. Inspection of figure 3 indicates that constituent bubbles oscillate as part of the ensemble and that the expansion and collapse phases are synonymous for both. The range of quiescent radii inferred from the RP model indicate that the frequency content within the acoustic emissions collected from the clouds originate from a source of radius comparable to that of the cloud, rather than that of the constituent bubbles. Taking the speed of sound in water as $1480\,\mathrm{m\,s^{-1}}$, implies a wavelength of $\lambda_0 \approx 2.7\,\mathrm{mm}$, for the HIFU frequency used in this work. As $\lambda_0 \gg R_0$, the quiescent radius required for the RP model, we conclude that this is a reasonable assumption for the purpose of analysing the acoustic emissions, in terms of scattered primary field. Further work is required to elucidate the role of individual bubbles within the ensemble, and their contribution to the acoustic radiation emitted, particularly through multi-bubble interaction models.

A HIFU PNP amplitude threshold for cloud response transitioning from a stable regime exhibiting $f_0/2$, into one of more pronounced nonlinearity with associated frequencies at $f_0/3$ and $2f_0/3$ is identified, in terms of the frequencies of the observed ensemble dynamics and in the acoustic emissions detected. The emitted frequencies may be fitted to existing models for bubble dynamics and information regarding the cloud size, relative to the driving frequency and pressure amplitude of insonation, extracted.

This work demonstrates that cavitation clouds can be characterized in terms of signature acoustic emissions, which could potentially be translated for monitoring of cavitation-mediated drug delivery from the vasculature, for focused ultrasound therapy. Tissue represents a much more inhomogeneous and viscoelastic host medium than the one used for this work. However, cavitation activity in blood vessels, from microbubbles delivered intravenously for example, may undergo similar evolution on HIFU exposure. In future work, we will employ the techniques reported to develop cloud manipulation strategies through HIFU duty cycle and intensity modulation, via rapid feedback-control loops detecting at signature frequencies, such as those identified.

Acknowledgments

This work was supported by TENOVUS Scotland and European Regional Development Funding. BG was supported by an Engineering and Physical Science Research Council (EPSRC, UK) DTA award. We are very grateful to the EPSRC instrument loan pool, notably Mr Adrian Walker, for access to high-speed imaging devices. We also acknowledge Oleg Prus and Javier Grinfeld of InSightec Ltd, Professors Andreas Melzer and Sandy Cochran of IMSaT, University of Dundee, and Professor Yoav Medan of Technion, Haifa Israel, for support and technical discussions.

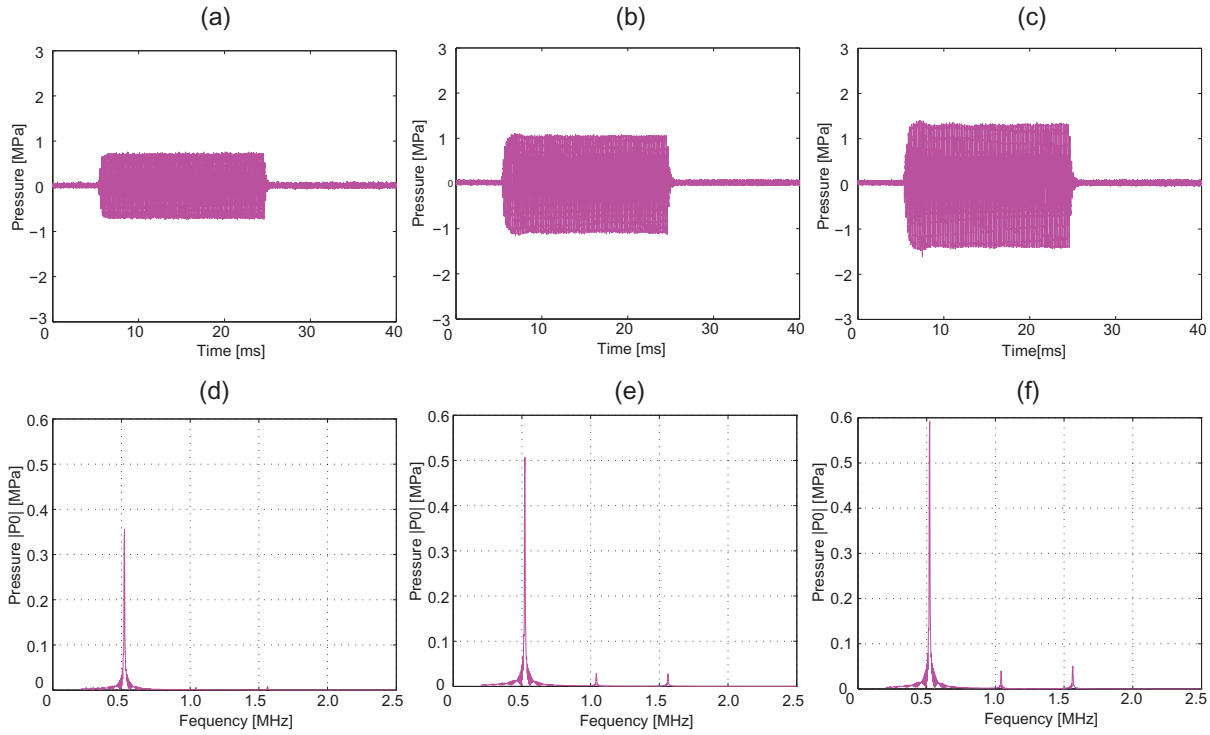

Figure A.1. Pressure measurements recorded at the HIFU focus at PNP amplitude of (a) 0.72, (b) 1.04 and (c) 1.29 MPa. (d)–(f) Associated amplitude spectra from 0 to 2.5 MHz after FFT.

Appendix. Assumption of HIFU nonlinearity

The expression used for the HIFU excitation, equation (2), assumes a linear monochromatic wave. It is well known that ultrasound at therapeutic intensities is often nonlinear with potentially strong high frequency harmonic components [24]. In terms of cavitation dynamics, these additional components may result in extraneous oscillations that need to be eliminated as a possible mechanism for the ensemble response observations reported.

Here, we present analysis of the HIFU field for nonlinear components and justify the assumption of linearity for the HIFU expression, by factoring high frequency terms into the RP model at the experimentally determined levels. Figures A.1(a)–(c) are *in situ* fibre-optic hydrophone recordings of HIFU bursts representative of those used to excite cavitation activity, at PNP = 0.72, 1.04 and 1.29 MPa, representative of the range used in this work. Cursory inspection indicates that the positive pressure amplitude is of approximately the same magnitude as the negative pressure amplitude, commonly taken as an indication of linearity. Figures A.1(d)–(f) are the associated amplitude spectra in the frequency domain, generated by FFT implementation, which reveal slight higher frequency components exist at $2f_0$ and $3f_0$, increasing for the larger pressure amplitudes as might be expected.

We demonstrate that the harmonic components do not have a significant effect on the model oscillation dynamics, by modifying equation (2) of the main manuscript to include higher

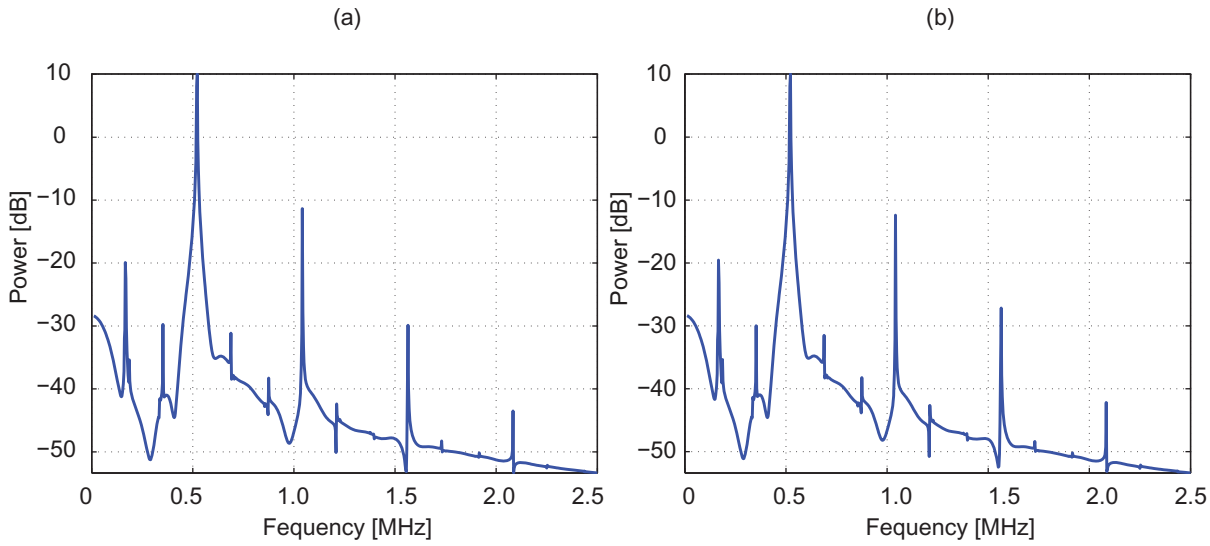

Figure A.2. RP model spectra for bubble oscillations HIFU of PNP = 1.29 MPa (a) under a linear approximation of HIFU, according to equation (2) of the main manuscript and (b) incorporating higher frequency harmonic components via equation (A.1) above, according to the spectrum of figure A.1(f).

frequency terms at the level recorded in the spectra of figures A.1(d)–(f), according to

$$P(t) = \sum_n a_n P_0 \sin(2\pi n f_0 t), \tag{A.1}$$

where n denotes the harmonic and a_n is a scaling factor representing the amplitude of the component. Implementing the RP model with equation (A.1) as the excitation expression, in a HIFU field of PNP = 1.29 MPa (the highest pressure amplitude used, and therefore most nonlinear HIFU generated) for the fundamental frequency $f_0 = 0.521$ MHz yields the bubble-oscillation spectrum of figure A.2(b). Also included as figure A.2(a), is the equivalent spectrum without the higher frequency harmonic components, as applicable for the linear approximation. Comparison of the spectra indicates that the higher frequency harmonic components of the nonlinear HIFU have no discernible influence on the sub-fundamental peaks in the model bubble oscillations, which match the experimentally detected frequency content of the cloud acoustic emissions. As such, we conclude that the observed frequency splitting in the model oscillation are due to the single bubble itself entering a regime of more pronounced nonlinearity at higher driving pressure amplitudes. We attribute the minimal influence of the harmonics to be due to the relatively small associated amplitudes, and that the higher frequencies are further from resonance with the selected values of R_0 for the model single bubbles.

References

[1] Suslick K S 1990 Sonochemistry *Science* **247** 1439–45
[2] McNamara W B, Didenko Y T and Suslick K S 1999 Sonoluminescence temperatures during multi-bubble cavitation *Nature* **401** 772–5
[3] Lamminen M O, Walker H W and Weavers L K 2004 Mechanisms and factors influencing the ultrasonic cleaning of particle-fouled ceramic membranes *J. Membr. Sci.* **237** 213–23

[4] Leighton T G 1994 *The Acoustic Bubble* (London: Academic)
[5] Lauterborn W and Cramer E 1981 Subharmonic route to chaos observed in acoustics *Phys. Rev. Lett.* **47** 1445–48
[6] Parlitz U, Englisch V, Scheffczyk C and Lauterborn W 1990 Bifurcation of bubble oscillators *J. Acoust. Soc. Am.* **88** 1061–77
[7] Lauterborn W and Kurz T 2010 Physics of bubble oscillations *Rep. Prog. Phys.* **73** 106501
[8] Tervo J T, Mettin R and Lauterborn W 2006 Bubble cluster dynamics in acoustic cavitation *Acta Acust.* **92** 178–80
[9] Yasui K, Iida Y, Tuziuti T, Kozuka T and Towata A 2008 Strongly interacting bubbles under an ultrasonic horn *Phys. Rev.* E **77** 016609
[10] Birkin P R, Offin D G, Vian C J B and Leighton T G 2011 Multiple observations of cavitation cluster dynamics close to an ultrasonic horn tip *J. Acoust. Soc. Am.* **130** 3379–88
[11] Coussios C C, Farny C H, ter Haar G R and Roy R 2007 Role of acoustic cavitation in the delivery and monitoring of cancer treatment by high-intensity focused ultrasound (HIFU) *Int. J. Hyperth.* **23** 105–20
[12] Bazan-Pergrino M, Arvanitis C D, Bassel R, Seymour L W and Coussios C C 2012 Ultrasound-induced cavitation enhances the delivery and therapeutic efficiency of an oncolytic virus in an *in vitro* model *J. Control. Release* **157** 235–42
[13] O'Reilly M A and Hynynen K 2012 Blood-brain barrier: real-time feedback-controlled focused ultrasound disruption by using an acoustic emissions-based controller *Radiology* **263** 96–106
[14] Gerold B, Kotopoulis S, McDougall C, McGloin D, Postema M and Prentice P 2011 Laser-nucleated acoustic cavitation in focused ultrasound *Rev. Sci. Instrum.* **82** 044902
[15] Vogel A, Busch S and Parlitz U 1996 Shock wave emission and cavitation bubble generation by picosecond and nanosecond optical breakdown in water *J. Acoust. Soc. Am.* **100** 148–65
[16] Gerold B, Glynne-Jones P, McDougall C, McGloin D, Cochran S, Melzer A and Prentice P 2012 Directed jetting from collapsing cavities exposed to focused ultrasound *Appl. Phys. Lett.* **100** 024104
[17] Minnaert M 1933 On musical air-bubbles and the sound of running water *Phil. Mag.* **16** 235–48
[18] Mettin R, Akhatov I, Parlitz U, Ohl C D and Lauterborn W 1997 Bjerknes forces between small cavitation bubbles in a strong acoustic field *Phys. Rev.* E **56** 2924–31
[19] Lauterborn W and Bolle H 1975 Experimental investigations of cavitation-bubble collapse in neighborhood of a solid boundary *J. Fluid Mech.* **72** 391
[20] Bremond N, Arora M, Ohl C D and Lohse D 2006 Controlled multibubble surface cavitation *Phys. Rev. Lett.* **96** 224501
[21] Plesset M S and Prosperetti A 1977 Bubble dynamics and cavitation *Annu. Rev. Fluid Mech.* **9** 145–85
[22] Segur J B and Oberstar H E 1951 Viscosity of glycerol and its aqueous solutions *Indust. Eng. Chem.* **49** 2117–20
[23] Rosenson R S, McCormick A and Uretz E F 1996 Distribution of blood viscosity values and biochemical correlates in healthy adults *Clin. Chem.* **42** 1189–95
[24] Muir T G and Carstensen E L 1980 Prediction of non-linear acoustic effects at biomedical frequencies and intensities *Ultrasound Med. Biol.* **6** 345–57